

A Stochastic Model for Colloid Transport and Deposition

S. A. Bradford* USDA-ARS

N. Toride Mie University

Profiles of retained colloids in porous media have frequently been observed to be hyper-exponential or non-monotonic with transport depth under unfavorable attachment conditions, whereas filtration theory predicts an exponential profile. In this work we present a stochastic model for colloid transport and deposition that allows various hypotheses for such deviations to be tested. The model is based on the conventional advective dispersion equation that accounts for first-order kinetic deposition and release of colloids. One or two stochastic parameters can be considered in this model, including the deposition coefficient, the release coefficient, and the average pore water velocity. In the case of one stochastic parameter, the probability density function (PDF) is characterized using log-normal, bimodal log-normal, or a simple two species/region formulation. When two stochastic parameters are considered, then a joint log-normal PDF is employed. Simulation results indicated that variations in the deposition coefficient and the average pore water velocity can both produce hyper-exponential deposition profiles. Bimodal formulations for the PDF were also able to produce hyper-exponential profiles, but with much lower variances in the deposition coefficient. The shape of the deposition profile was found to be very sensitive to the correlation of deposition and release coefficients, and to the correlation of pore water velocity and deposition coefficient. Application of the developed stochastic model to a particular set of colloid transport and deposition data indicated that chemical heterogeneity of the colloid population could not fully explain the observed behavior. Alternative interpretations were therefore proposed based on variability of the pore size and the water velocity distributions.

COLLOID deposition in porous media has typically been quantified using clean-bed filtration theory (e.g., Logan et al., 1995; Tufenkji and Elimelech, 2004a). This theory invokes a first-order colloid attachment term, which produces an exponential spatial distribution of retained colloids. Over the past decade a growing body of literature indicates that clean-bed filtration theory frequently does not provide an accurate characterization of experimental deposition profiles under unfavorable (when repulsive electrostatic interactions exist between the colloids and grain surfaces) attachment conditions (Camesano and Logan, 1998; Bolster et al., 1999; Redman et al., 2001; Bradford et al., 2002; Tufenkji et al., 2003; Li et al., 2004; Tufenkji and Elimelech, 2005a, 2005b). In this case, retained colloids frequently exhibit a depth-dependent deposition rate which produces hyper-exponential (a decreasing rate of deposition with increasing distance) (Albinger et al., 1994; DeFlaun et al., 1997; Baygents et al., 1998; Simoni et al., 1998; Bolster et al., 2000; Zhang et al., 2001; Redman et al., 2001; Bradford et al., 2002; Li et al., 2004; Bradford and Bettahar, 2005) or non-monotonic (a peak in retained colloids away from the injection source) (Tong et al., 2005; Bradford et al., 2006b) deposition profiles. Experimental deposition profiles for larger colloids and finer textured porous media have also been reported to be less consistent with exponential profiles that are predicted by filtration theory (Bradford et al., 2003; Tufenkji and Elimelech, 2005a).

A variety of explanations for the observed deviations from filtration theory predictions have been proposed in the literature. Proposed chemical explanations include porous media charge variability (Johnson and Elimelech, 1995), heterogeneity in surface charge characteristics of colloids (Bolster et al., 1999; Li et al., 2004), deposition of colloids in the secondary energy minimum of the Derjaguin-Landau-Verwey-Overbeek (DLVO) interaction energy curves (Redman et al., 2004; Hahn et al., 2004; Tufenkji and Elimelech, 2005a), time-dependent attachment (Tan et al., 1994; Liu et al., 1995), and colloid detachment (Tufenkji et al., 2003). Other researchers have suggested that deposition may occur as a result of physical factors that are not included in filtration theory, such as straining (deposition of colloids in small pores such as those formed at grain-grain junctions) (Cushing and Lawler, 1998; Bradford et al., 2002, 2003, 2004, 2005, 2006a, 2006b; Li et al., 2004; Tufenkji et al., 2004; Bradford and Bettahar, 2005; Foppen et al., 2005), soil surface roughness (Kretzschmar et al., 1997; Redman et al., 2001), and hydrodynamic drag (Li et al., 2005).

Various mathematical models have been formulated to characterize hyper-exponential and non-monotonic deposition profiles and associ-

Copyright © 2007 by the American Society of Agronomy, Crop Science Society of America, and Soil Science Society of America. All rights reserved. No part of this periodical may be reproduced or transmitted in any form or by any means, electronic or mechanical, including photocopying, recording, or any information storage and retrieval system, without permission in writing from the publisher.

Published in *J. Environ. Qual.* 36:1346–1356 (2007).

doi:10.2134/jeq2007.0004

Received 1 Jan. 2007.

*Corresponding author (sbradford@usrl.ars.usda.gov).

© ASA, CSSA, SSSA

677 S. Segoe Rd., Madison, WI 53711 USA

S.A. Bradford, USDA-ARS, United States Salinity Lab., 450 W. Big Springs Rd., Riverside, CA 92507-4617. N. Toride, Faculty of Bioresources, Mie Univ., 1577 Kurimamachiya-cho Tsu, Japan, 514-8507.

ated colloid breakthrough curves (Bradford et al., 2003, 2006b; Tufenkji et al., 2003; Tufenkji and Elimelech, 2004b, 2005a, 2005b; Li et al., 2004). In particular, stochastic models have been used to account for chemical heterogeneity of colloid and grain surfaces on colloid deposition in column-scale studies (Tufenkji et al., 2003; Tufenkji and Elimelech, 2004b, 2005a, 2005b; Li et al., 2004). In these works various probability density functions for the colloid attachment coefficient have been proposed (Tufenkji et al., 2003) and utilized to characterize hyperexponential deposition profiles. Differences in the stochastic modeling approaches for colloid deposition include the selected attachment coefficient probability density function and the solution technique of the governing transport equation (steady-state analytical solution that neglects dispersion or using a transient transport particle tracking algorithm). Other stochastic models for colloid transport that have appeared in the literature have focused on large-scale transport behavior in heterogeneous systems (Rehmann et al., 1999; Maxwell et al., 2003; Bekhit and Hassan, 2005).

The objective of this work is to present the development and utilization of a stochastic model for colloid transport and deposition. Published research has only provided a limited discussion of the physical and/or chemical basis for selected probability density functions that describe colloid attachment. Furthermore, alternative explanations for fitted deposition coefficient distributions such as variations in the colloid size, the pore size, and the velocity distributions have not been discussed. In this work we attempt to utilize deposition coefficient distributions that are consistent with measured colloid or porous medium properties. Furthermore, stochastic models provide an opportunity to study the effects of coupling of several stochastic variables on colloid transport and deposition processes. This includes the potential interactions of colloid deposition and release coefficients with each other and with water velocity.

Colloid Transport Model

The CXTFIT program (Toride et al., 1995) is the foundation for our stochastic modeling effort. This code includes the analytical solution for the one-dimensional advective dispersion equation with one-site kinetic chemical nonequilibrium deposition subject to various initial and boundary conditions. This model formulation is equivalent to the well-known first-order attachment and detachment model that is commonly employed to describe colloid transport and deposition (e.g., Harvey and Garabedian, 1991; Corapcioglu and Choi, 1996; Bolster et al., 1999; Schijven and Hassanizadeh, 2000). This analytical solution is used in conjunction with the stochastic stream tube model in CXTFIT to explore colloid transport and deposition. Jury and Roth (1990) provide additional information on assumptions that are employed in the stochastic stream tube model. Relevant aspects of this code and specific model adaptations are discussed below.

Deterministic Colloid Transport and Deposition

When the volumetric water content and flux remain constant in time (steady-state water flow), the aqueous phase mass balance equation for colloids can be written as:

$$\frac{\partial C}{\partial t} = D \frac{\partial^2 C}{\partial z^2} - v \frac{\partial C}{\partial z} - k_d C + \frac{\rho_b k_r}{\theta_w} S \quad [1]$$

where C ($N_c L^{-3}$; N_c and L denotes the number of colloids and length, respectively) is the colloid concentration in the aqueous phase, t (T) is time, z (L) is depth, D is the hydrodynamic dispersion coefficient ($L^2 T^{-1}$), v is the average pore water velocity ($L T^{-1}$), ρ_b ($M L^{-3}$; M denotes mass) is the soil bulk density, S ($N_c M^{-1}$) is the solid phase concentration of the retained colloids, θ_w (–) is the volumetric water content, and k_d (T^{-1}) and k_r (T^{-1}) are the first-order colloid deposition and release coefficients, respectively. The corresponding colloid mass balance equation for the solid phase is given as:

$$\frac{\rho_b}{\theta_w} \frac{\partial S}{\partial t} = k_d C - \frac{\rho_b k_r}{\theta_w} S \quad [2]$$

Clean bed attachment is assumed and filtration theory is incorporated into the k_d term of Equations [1] and [2] when $k_r = 0$ (e.g., Yao et al., 1971; Logan et al., 1995) as:

$$k_d = \frac{3(1-\theta_w)}{2d_{50}} \eta \alpha v \quad [3]$$

where η (–) is the collector (porous medium) efficiency, α (–) is the colloid sticking efficiency, and d_{50} (L) is the median porous medium grain diameter. The collector efficiency accounts for the mass flux of colloids to the collector surface via diffusion, interception, and gravitational sedimentation and is defined as the ratio of the total colloid flux which strikes the collector (grain surface) to the rate at which particles flow toward the collector (Yao et al., 1971). The value of η is frequently calculated using correlations written in terms of dimensionless variables (e.g., Rajagopalan and Tien, 1976; Logan et al., 1995; Tufenkji and Elimelech, 2004a). The sticking efficiency is defined as the ratio of the deposition flux under unfavorable relative to favorable conditions. The value of α is typically assumed to depend on the surface chemistries of the colloids and the grain surfaces (Ryan and Elimelech, 1996), and to be independent of the water velocity and the size of the colloid and the collector because these factors are accounted for by η in Eq. [3]. In practice α is usually derived from experimental breakthrough curves, or from fitted values of k_d and calculated values of η , although theoretical approaches have also been proposed to predict α (Simoni et al., 1998; Ryan et al., 1999; Dong et al., 2002).

One Stochastic Variable

The value of k_d that is found in Eq. [1–3] is typically assumed to be constant. In the stochastic modeling approach, parameters may be defined by probability density functions. If k_d is considered to be stochastic, we assume a log-normal probability density function (PDF) that is defined as:

$$F(k_d) = \frac{1}{k_d \sigma_d \sqrt{2\pi}} \exp\left[-\frac{Y_d^2}{2}\right] \quad [4]$$

where σ_d is the standard deviation of the log-normal

probability density function, and Y_d is the normalized log-transformed variable defined as:

$$Y_d = \frac{\ln(k_d) - \mu_d}{\sigma_d} \quad [5]$$

Here μ_d is the mean value of the log-normal probability density function defined as $\mu_d = \ln(\langle k_d \rangle) - 0.5\sigma_d^2$, where $\langle k_d \rangle$ is the ensemble average of k_d . The subscript d is used on σ_d , Y_d , and μ_d to identify parameters associated with the deposition coefficient. Subscripts r and v are used in a similar fashion to identify parameters associated with the release coefficient and the pore water velocity, respectively.

The mean aqueous and solid phase colloid concentrations at a given depth and time can be determined for various functional forms of $F(k_d)$ as:

$$\langle C(z, t) \rangle = \int_0^\infty C(z, t; k_d) F(k_d) dk_d \quad [6]$$

and

$$\langle S(z, t) \rangle = \int_0^\infty S(z, t; k_d) F(k_d) dk_d \quad [7]$$

where $C(z, t; k_d)$ and $S(z, t; k_d)$ are aqueous and solid phase colloid concentrations determined from the analytical solution of Eq. [1] and [2]. The variance in aqueous and solid phase colloid concentrations can also be calculated using this stochastic modeling approach (e.g., Toride et al., 1995). For example, the variance of $S(z, t)$ is given as $\langle S(z, t)S(z, t) \rangle - \langle S(z, t) \rangle^2$. If v is stochastic and k_d is constant, Eq. [4–7] can be rewritten by replacing k_d with v , σ_d with σ_v , Y_d with Y_v , and μ_d with μ_v .

As an alternative to Eq. [4], bimodal log-normal distributions may be employed to behave more complex transport and deposition behavior (Tufenkji et al., 2003) as:

$$F(k_d) = \frac{f_1}{k_{d1}\sigma_{d1}\sqrt{2\pi}} \exp\left[-\frac{Y_{d1}^2}{2}\right] + \frac{(1-f_1)}{k_{d2}\sigma_{d2}\sqrt{2\pi}} \exp\left[-\frac{Y_{d2}^2}{2}\right] \quad [8]$$

Here f_1 denotes the fraction of k_d that is assigned to log-normal distribution 1. Subscripts 1 and 2 are included on σ_{d1} , Y_{d1} , and μ_{d1} and $\langle k_d \rangle$ to identify the two log-normal distributions. When σ_{d1} and σ_{d2} approach zero values, $F(k_d)$ that is given by Eq. [8] can be approximated by the following simple functional form:

$$F(k_d) = f_1\delta(k_d - k_{d1}) + (1-f_1)\delta(k_d - k_{d2}) \quad [9]$$

where δ is the Dirac delta function, and k_{d1} and k_{d2} are used to distinguish the two deposition coefficients. Equations [8] and [9] can both be used in Eq. [6] and [7] to determine $\langle C(z, t) \rangle$ and $\langle S(z, t) \rangle$. When using Eq. [9], however, the stochastic model for k_d (Eq. [6–7]) reduces to the following simple equations:

$$\langle C(z, t) \rangle = f_1 C(z, t; k_{d1}) + (1-f_1) C(z, t; k_{d2}) \quad [10]$$

and

$$\langle S(z, t) \rangle = f_1 S(z, t; k_{d1}) + (1-f_1) S(z, t; k_{d2}) \quad [11]$$

Two Stochastic Variables

If both k_d and k_r are assumed to be log-normal stochastic parameters that are correlated, then a joint probability density function is defined as:

$$F(k_d, k_r) = \frac{1}{2\pi\sigma_d\sigma_r k_d k_r \sqrt{1-\rho_{dr}^2}} \exp\left[-\frac{Y_r^2 - 2\rho_{dr}Y_r Y_d + Y_d^2}{2(1-\rho_{dr}^2)}\right] \quad [12]$$

The parameter ρ_{dr} is the correlation coefficient between Y_d and Y_r and is defined as:

$$\rho_{dr} = \langle Y_d Y_r \rangle = \int_0^\infty \int_0^\infty Y_r Y_d F(k_d, k_r) dk_d dk_r \quad [13]$$

When Y_d and Y_r are perfectly correlated then $\rho_{dr} = 1$, when they are uncorrelated $\rho_{dr} = 0$, and when they are perfectly inversely correlated $\rho_{dr} = -1$.

The mean aqueous and solid phase colloid concentrations at a given depth and time can also be determined for two log-normally distributed parameters k_d and k_r as:

$$\langle C(z, t) \rangle = \int_0^\infty \int_0^\infty C(z, t; k_d, k_r) F(k_d, k_r) dk_d dk_r \quad [14]$$

and

$$\langle S(z, t) \rangle = \int_0^\infty \int_0^\infty S(z, t; k_d, k_r) F(k_d, k_r) dk_d dk_r \quad [15]$$

where $C(z, t; k_d, k_r)$ and $S(z, t; k_d, k_r)$ are again the aqueous and solid phase colloid concentrations determined from the analytical solution of Eq. [1] and [2]. The variance in solid phase colloid concentrations is again given as $\langle S(z, t)S(z, t) \rangle - \langle S(z, t) \rangle^2$ when using the two parameter stochastic model. Alternatively, if k_d and v are stochastic and k_r is constant, Eq. [12–15] can be rewritten by replacing k_r and v .

Example Simulations

In this section we present illustrative examples of colloid transport and deposition for the various stochastic models. Break-through curves (at a depth of 10 cm) are plotted herein with the relative flux concentrations on the y axis and time on the x axis. When v is constant, the relative flux concentration is equal to $\langle C \rangle / C_i$ where C_i ($N_{ic} L^{-3}$; N_{ic} is the number of colloids in a unit volume of C_i) is the initial colloid concentration in the influent suspension. In contrast, when v is stochastic the relative flux concentration is defined as $\langle vC \rangle / (\langle v \rangle C_i)$ and the amount of colloids added to a given stream tube is dependent on the velocity of the stream tube. Additional details are given in Toride et al. (1995) on the determination of flux concentrations. Final deposition profiles (after 250 minutes) are plotted herein with the normalized solid phase colloid concentration, defined as $\langle S \rangle / N_{ic}$, on the x axis and distance from the column inlet on the y axis. A third-type bound-

ary condition was used at the inlet, and a concentration gradient of zero was fixed at z equal to infinity. The initial concentration in the simulation domain was zero. The colloid pulse duration in all cases was 75 min. Other input model parameters for the simulations presented in this section are provided in the figure captions.

Figure 1 presents colloid breakthrough curves (Fig. 1a) and deposition profiles (Fig. 1b) when k_d is stochastic and the value of σ_d from the log-normal probability density function (Eq. [4]) is 0, 0.5, and 1.0. Trends in Fig. 1 can be explained by differences in the probability density function. When $\sigma_d = 0$ the stochastic model reduces to the conventional first-order attachment-detachment model, and the deposition profile (Fig. 1b) is very close to exponential with depth because k_r is low (0.001 min^{-1}). In contrast, when σ_d increased, the spread of the log-normal distribution increased and the distribution became more asymmetric, with a greater frequency of low and high values of k_d . The value of $\langle k_d \rangle$ was always the same for the simulations presented in Fig. 1, but μ_d decreased with increasing σ_d . This produced higher effluent concentrations (Fig. 1a) and corresponding less deposition (Fig. 1b). The deposition profiles for the $\sigma_d > 0$ cases exhibited greater curvature near the sand surface than the $\sigma_d = 0$ simulation (Fig. 1b), and were therefore increasingly hyperexponential with increasing σ_d . This observation can be attributed to the variance of the deposited colloids, which was greatest near the column inlet and increased with increasing σ_d (Fig. 1c) due to higher values of k_d in the log-normal distribution. Conversely, as the distance of transport increased, the remaining colloids in solution were associated with lower values of k_d in the log-normal distribution that produced a lower variance of S/N_{ic} in Fig. 1c. Hence, the shape of the probability density function of mobile colloids in solution effectively became more uniform (the variance decreased) with increasing transport distance.

Figure 2 presents similar information as in Fig. 1, but for the case of stochastic v and constant k_d and k_r . In Fig. 2a increasing σ_v produced earlier breakthrough times, higher effluent concentrations, and the breakthrough curves tended to be more asymmetric. These observations can be explained by the increased spread in the velocity distribution, which produced a small fraction of faster stream tubes that transported most of the colloids. In Fig. 2b the deposition profiles become more hyperexponential (exhibited greater curvature near the surface than the exponential, $\sigma_v = 0$, case) as σ_v increased for similar reasons. The shape and magnitude of the deposition profiles in Fig. 1b and 2b were quite similar for identical variations in k_d or v . The variance of deposited colloids, however, was much lower for stochastic v (Fig. 2c) than stochastic k_d (Fig. 1c).

Figure 3 presents colloid breakthrough curves (Fig. 3a) and deposition profiles (Fig. 3b) when k_d is stochastic according to Eq. [8]. Specific parameter values for these simulations were $\sigma_{d1} = 0.1$, $\sigma_{d2} = 0.1$, $\langle k_{d1} \rangle = 0.015 \text{ min}^{-1}$, $\langle k_{d2} \rangle = 0.3 \text{ min}^{-1}$, and f_1 equal to 0, 0.25, 0.5, 0.75, and 1.0. As f_1 increased the effluent concentration increased and the amount of deposition decreased. Comparison of the simulation results shown in Fig. 1 and 3 suggest that much lower variances in k_d were needed to obtain hyperexponential profiles when using $F(k_d)$ described by Eq. [8] than Eq. [4]. In fact, variations in σ_{d1} and σ_{d2} had a relatively low impact on measured breakthrough curves and

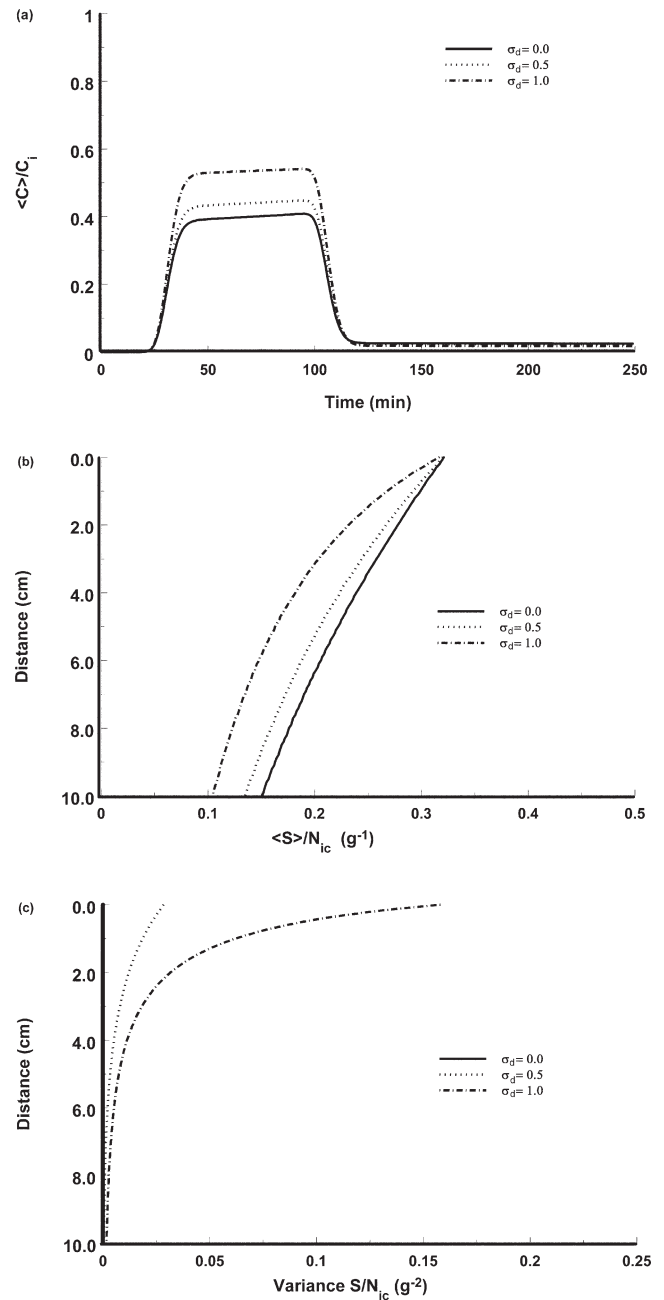


Fig. 1. (a) Plot of the relative flux concentration, $\langle C \rangle / C_i$, at a depth of 10 cm as a function of time when k_d is stochastic and the value of σ_d from the log-normal probability density function (Eq. [4]) is 0, 0.5, and 1.0. (b, c) Corresponding normalized solid phase colloid concentration, $\langle S \rangle / N_{ic}$, and associated variance after 250 min with depth, respectively. Model parameters that were employed in these simulations were $D = 0.0313 \text{ cm}^2 \text{ min}^{-1}$, $v = 0.313 \text{ cm min}^{-1}$, $\langle k_d \rangle = 0.03 \text{ min}^{-1}$, and $k_r = 0.001 \text{ min}^{-1}$.

deposition profiles compared with changes in f_1 . This observation indicates that Eq. [9–11] may be used as a relatively simple means of simulating hyperexponential deposition profiles.

Figure 4 presents colloid breakthrough curve (Fig. 4a) and deposition profiles (Fig. 4b) when k_d and k_r are both log-normal stochastic parameters and values of $\rho_{dr} = -1, -0.5, 0, 0.5$, and 1. Relevant model parameters for these simulations were $\langle k_d \rangle = 0.03 \text{ min}^{-1}$, $\langle k_r \rangle = 0.005 \text{ min}^{-1}$, $\sigma_d = 1$, and $\sigma_r = 1$. It is

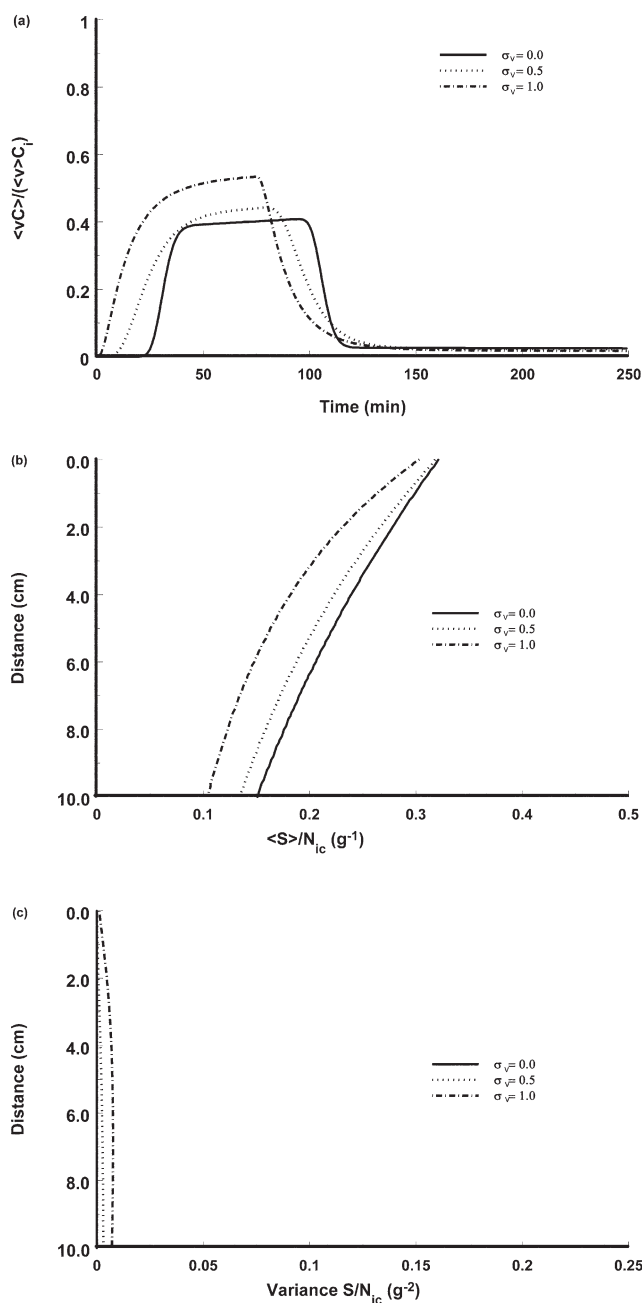


Fig. 2. (a) Plot of the relative flux concentration, $\langle vC \rangle / (\langle v \rangle C_i)$, at a depth of 10 cm as a function of time when v is stochastic and the value of σ_v from the log-normal probability density function (Eq. [4]) is 0, 0.5, and 1.0. (b, c) Corresponding normalized solid phase colloid concentration, $\langle S \rangle / N_{ic}$, and associated variance after 250 min with depth, respectively. Model parameters that were employed in these simulations were $D = 0.0313 \text{ cm}^2 \text{ min}^{-1}$, $\langle v \rangle = 0.313 \text{ cm min}^{-1}$, $k_d = 0.03 \text{ min}^{-1}$, and $k_r = 0.001 \text{ min}^{-1}$.

logical to anticipate that negative values of ρ_{dr} are more physically realistic than positive values, because they imply that sites with greater deposition rates retain colloids more strongly (less reversibly) than sites with lower deposition rates. Conversely, increasingly positive values of ρ_{dr} imply the opposite trend. Changes in ρ_{dr} had little influence on the early portion of the breakthrough curves. The concentration tailing portion of the breakthrough curves, however, was sensitive to values of ρ_{dr} .

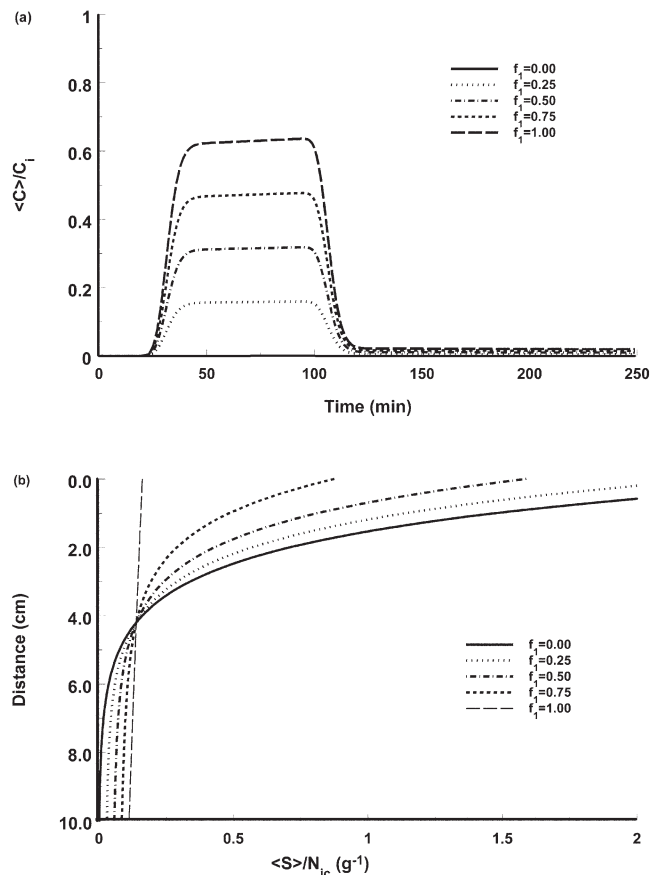


Fig. 3. (a) Plot of the relative flux concentration, $\langle C \rangle / C_i$, at a depth of 10 cm as a function of time when k_d is stochastic, the values of $\sigma_{d1} = 0.1$ and $\sigma_{d2} = 0.1$ from the bimodal log-normal probability density function (Eq. [8]), and f_i is equal to 0, 0.25, 0.5, 0.75, and 1. (b) Corresponding normalized solid phase colloid concentration, $\langle S \rangle / N_{ic}$, after 250 min with depth. Other model parameters that were employed in these simulations were $D = 0.0313 \text{ cm}^2 \text{ min}^{-1}$, $v = 0.313 \text{ cm min}^{-1}$, $\langle k_{d1} \rangle = 0.015 \text{ min}^{-1}$, $\langle k_{d2} \rangle = 0.3 \text{ min}^{-1}$, and $k_r = 0.001 \text{ min}^{-1}$.

with increased tailing occurring when $\rho_{dr} = 1.0$ because these deposited colloids were retained more weakly. The deposition profiles were very sensitive to values of ρ_{dr} . When $\rho_{dr} = -1.0$ the deposition profiles were more hyperexponential because retained colloids with the greatest deposition rates occur near the column inlet and were more strongly retained than those at greater transport distances. As ρ_{dr} increased from -1 to 0.5 the profiles became less hyperexponential (more uniform with depth), and $\rho_{dr} = 1$ produced a profile that was nonmonotonic. Although the values of σ_d and σ_r were the same in all the simulations, the variance of the deposited colloids after 250 min was highest for decreasing values of ρ_{dr} (Fig. 4c), especially near the column inlet. When $\rho_{dr} = -1$ the variability in the deposition profile was more persistent because these colloids were more strongly retained (less reversible) than when $\rho_{dr} = 1$.

Figure 5 presents colloid breakthrough curves (Fig. 5a) and deposition profiles (Fig. 5b) when v and k_d are both log-normal stochastic parameters and values of $\rho_{vd} = -1, -0.5, 0, 0.5, \text{ and } 1$. Other relevant model parameters for these simulations were $\langle v \rangle = 0.313 \text{ cm min}^{-1}$, $\langle k_d \rangle = 0.03 \text{ min}^{-1}$, $k_r = 0.001 \text{ min}^{-1}$, $\sigma_v = 1$, and $\sigma_d = 1$. Decreasing values of ρ_{vd} imply that higher transport veloci-

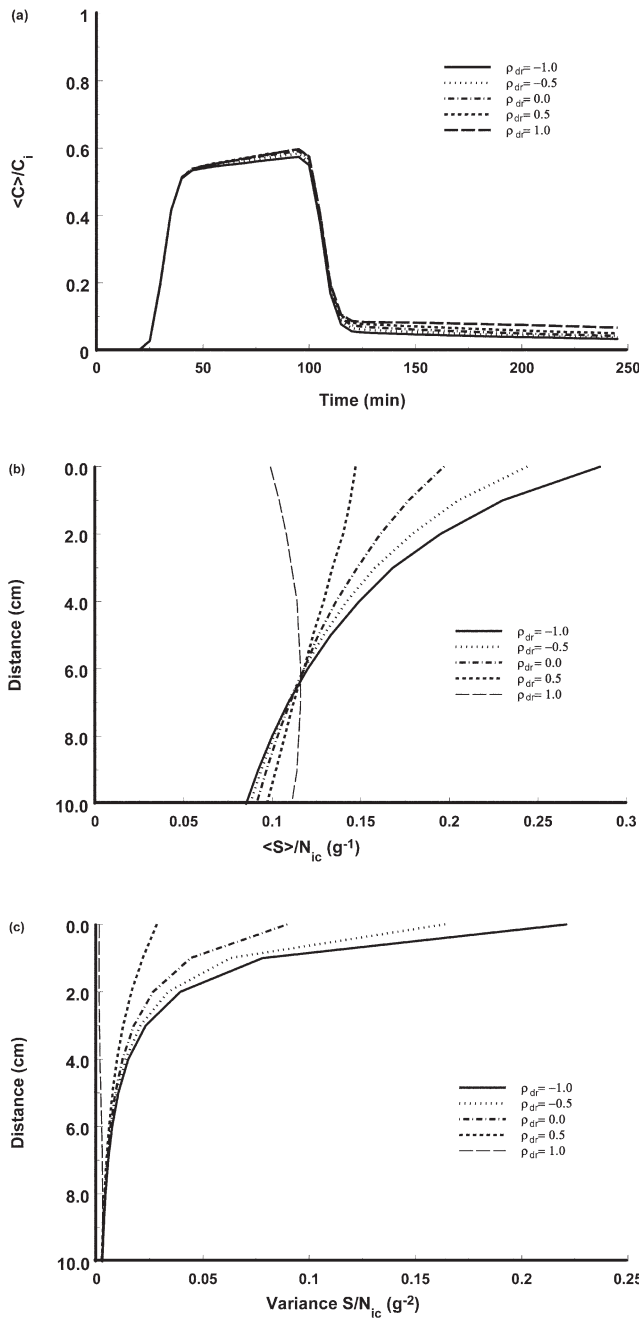


Fig. 4. (a) Plot of the relative flux concentration, $\langle C \rangle / C_i$ at a depth of 10 cm as a function of time when k_d and k_r are both stochastic parameters and values of $\rho_{dr} = -1, -0.5, 0, 0.5,$ and 1 . (b, c) Corresponding normalized solid phase colloid concentration, $\langle S \rangle / N_{ic}$ and associated variance after 250 min with depth, respectively. Model parameters that were employed in these simulations were $D = 0.0313 \text{ cm}^2 \text{ min}^{-1}$, $v = 0.313 \text{ cm min}^{-1}$, $\langle k_d \rangle = 0.03 \text{ min}^{-1}$, $\langle k_r \rangle = 0.005 \text{ min}^{-1}$, $\sigma_d = 1$, and $\sigma_r = 1$.

ties are associated with lower deposition rates. Negative values of ρ_{vd} are believed to be more physically realistic than positive values of ρ_{vd} because recent experimental evidence demonstrates that the value of α in Eq. [3] decreased with increasing water velocity under unfavorable attachment conditions (Tong et al., 2005; Johnson et al., 2006). Decreasing ρ_{vd} in Fig. 5a produced higher effluent concentrations and less concentration tailing. In Fig. 5b when

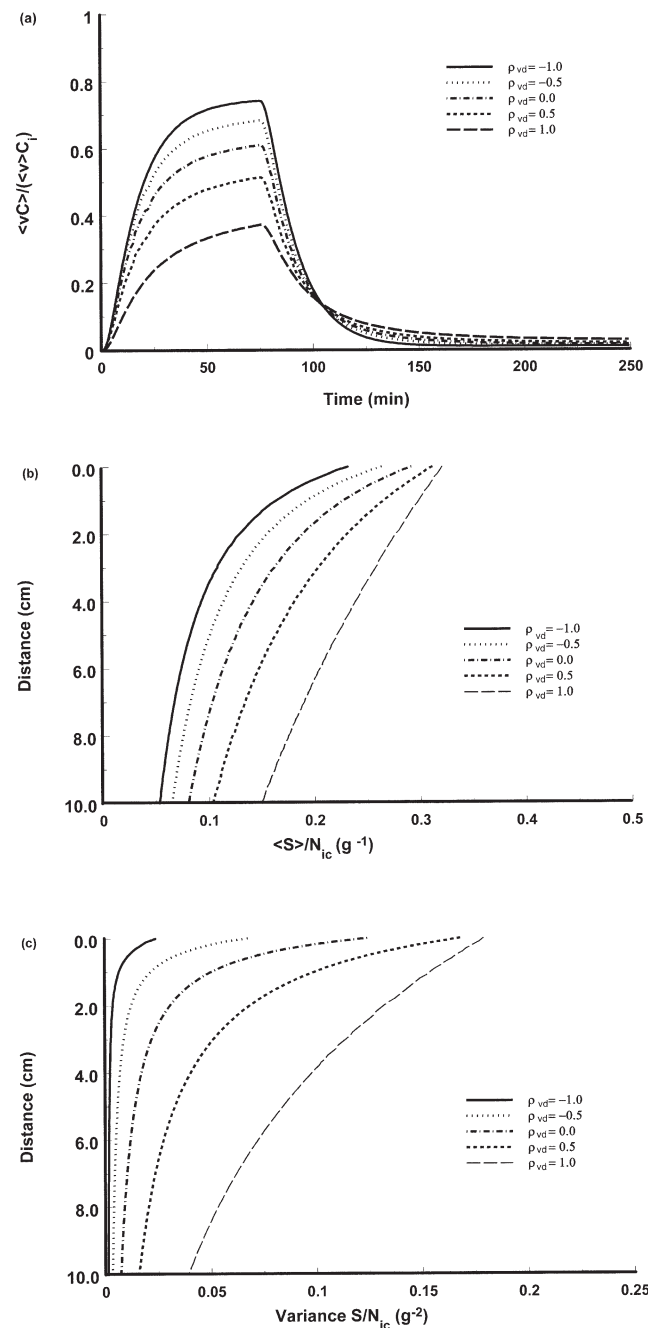


Fig. 5. (a) Plot of the relative flux concentration, $\langle vC \rangle / (\langle v \rangle C_i)$, at a depth of 10 cm as a function of time when v and k_d are both stochastic parameters and values of $\rho_{vd} = -1, -0.5, 0, 0.5,$ and 1 . (b, c) Corresponding normalized solid phase colloid concentration, $\langle S \rangle / N_{ic}$ and associated variance after 250 min with depth, respectively. Model parameters that were employed in these simulations were $D = 0.0313 \text{ cm}^2 \text{ min}^{-1}$, $\langle v \rangle = 0.313 \text{ cm min}^{-1}$, $\langle k_d \rangle = 0.03 \text{ min}^{-1}$, $k_r = 0.001 \text{ min}^{-1}$, $\sigma_v = 1$, and $\sigma_d = 1$.

$\rho_{vd} = -1.0$ the deposition profiles were more hyperexponential because retained colloids with the greatest deposition rates occurred near the column inlet and were associated with lower flow rates. Similar to Fig. 4c the variance of deposited colloids in Fig. 5c tended to be highest near the column inlet. In this case, however, higher variances in the deposited colloids occurred with increasing

values of ρ_{vd} . Relatively low variances were associated with the $\rho_{vd} = -1.0$ system that produced the most hyperexponential profile.

Application and Discussion

Previous application of stochastic colloid transport and deposition models that have appeared in the literature have used various functional forms for $F(k_d)$ to describe measured colloid

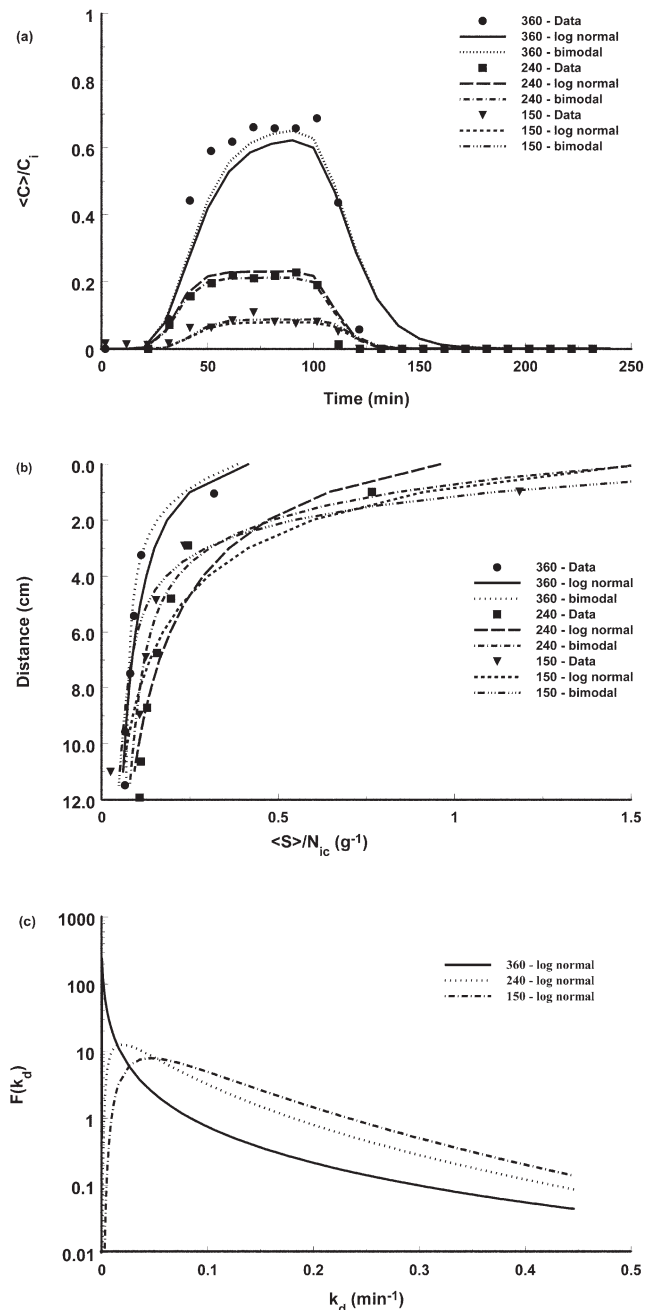


Fig. 6. (a) Plot of the observed and simulated relative flux concentration, $\langle C \rangle / C_i$, at a depth of 12 cm for 3 μm carboxyl modified latex colloids in quartz sands having median grain sizes of 360, 240, and 150 μm . (b) Corresponding observed and simulated normalized solid phase colloid concentration, $\langle S \rangle / N_{ic}$, after 250 min with depth. Simulations considered log-normal (Eq. [4]) and bimodal (Eq. [9]) formations for $F(k_d)$. (c) Log-normal values of $F(k_d)$. Table 1 provides a summary of measured and/or fitted model parameters.

transport and deposition data (Bolster et al., 1999; Tufenkji et al., 2003; Li et al., 2004; Tufenkji and Elimelech, 2005b). Variations in porous media and/or colloid surface charge have frequently been invoked as a potential explanation for nonexponential deposition profiles. Differences in mineralogy and/or the presence of coatings of metal oxides or organic matter are expected to produce variations in surface charge (Davis, 1982; Tipping and Cooke, 1982; Song and Elimelech, 1993, 1994). Johnson and Li (2005), however, demonstrated that porous media charge variability and/or the influence of the DLVO secondary energy minimum should theoretically be consistent with an exponential deposition profile. The hypothesis of colloid charge variability has been invoked for a variety of colloids, including microorganisms (Simoni et al., 1998) and latex microspheres (Li et al., 2004; Tufenkji and Elimelech, 2005b; Tong and Johnson, 2007). Variations in surface charge of microorganisms can occur as a result of differences in growth stage, metabolic activity, and genetic differences. In contrast, latex microspheres are typically highly uniform and exhibit small variations in zeta potential.

Figures 6a and 6b present observed and simulated breakthrough curves and deposition profiles, respectively, for 3 μm carboxyl modified latex colloids in quartz sands having median grain sizes of 360, 240, and 150 μm . A short summary of relevant experimental conditions and protocols is provided below before discussing this transport data. The ionic strength of the colloid suspension was 6 mM and the pH was buffered to 10 using 1.7 mM $NaHCO_3$ and 1.7 mM Na_2CO_3 to minimize the potential for colloid and porous media charge variability. The zeta potential of these colloids was measured with a ZetaPals instrument (Brookhaven Instruments Corporation, Holtsville, NY) to be -76.3 ± 3.48 mV (± 2 standard deviations). The zeta potential for quartz sands in low ionic strength solution at a pH of 10 has been reported to be approximately -80 mV (Elimelech et al., 2000).

The colloid suspension was pumped upward through the vertically oriented saturated columns (4.8 cm inside diameter and 13 cm in length) at a steady pore water velocity of around 0.3 $cm\ min^{-1}$; after 75 min a three-way valve was used to switch to eluant solution of the same solution chemistry for an additional 175 min (total of 250 minutes). Effluent samples were collected and analyzed for colloid concentration using a Turner Quantech Fluorometer (Barnstead/ThermoLyne, Dubuque, IA). Following completion of the colloid transport experiments, the spatial distribution of retained colloids in each packed column was determined by excavating the sand into tubes containing excess eluant solution, slowly shaking the tubes for 15 min, and measuring the concentration of the colloids in the excess solution with the fluorometer. A detailed discussion of the experimental conditions and protocols is given in Bradford et al. (2002, 2007).

Simulations shown in Fig. 6a and 6b considered log-normal (Eq. [4]) and bimodal (Eq. [9]) formations for $F(k_d)$. Figure 6c presents a plot of the fitted values of the log normal $F(k_d)$ for these systems. Table 1 provides the fitted stochastic model parameters $\langle k_d \rangle$ and σ_d from Eq. [4], and the coefficient of linear regression to effluent (r_{eff}^2) and deposition (r_{sand}^2) data. Observe that both breakthrough curves and deposition profiles are fairly well

described using the stochastic model with the log-normal probability density function, but values of σ_d are very high (Table 1).

In case of unfavorable attachment conditions (experiments were conducted at pH = 10) an upper limit on the value of α can be estimated using the following expression (Simoni et al., 1998):

$$\alpha = \int_0^{-\Phi_2} \frac{2}{k_b T_k} \left(\frac{E}{\pi k_b T_k} \right)^{0.5} \exp\left(-\frac{E}{k_b T_k}\right) dE = \frac{\Gamma_i(1.5, -\Phi_2)}{\Gamma(1.5)} \quad [16]$$

where E ($M L^2 T^{-2}$) is the kinetic energy of diffusing colloids that follow a Maxwell distribution, T_k ($^{\circ}K$; where $^{\circ}K$ is temperature in degrees Kelvin) is the temperature, k_b ($M L^2 T^{-2} K^{-1}$) is the Boltzmann constant, Φ_2 (-) is the depth of the secondary energy minimum of the DLVO interaction energy profile (normalized by $k_b T_k$), Γ_i is the incomplete gamma function, and Γ is the gamma function. The above analysis neglects the potential role of hydrodynamics on colloid deposition and is therefore only an upper limit on α . Dong et al. (2002) reported, however, that Eq. [16] provided a good prediction of measured values of α .

The value of Φ_2 in Eq. [16] can be determined from measured values of zeta potential for a given colloid suspension and porous medium using DLVO theory (Derjaguin and Landau, 1941; Verwey and Overbeek, 1948; Hogg et al., 1966; Gregory, 1981). A value of 4.04×10^{-21} J for the Hamaker constant was assumed to represent our polystyrene latex-water-quartz system in these calculations (Bergendahl and Grasso, 1999). If the 95% confidence interval is known for colloid and/or porous media zeta potentials, then the corresponding 95% confidence interval on Φ_2 , α (Eq. [16]), and k_d (Eq. [3]) can be determined. When using measured values of the colloid zeta potential (-76.3 ± 3.48 mV) and literature values (Elimelech et al., 2000) for the quartz zeta potential (-80 mV), the calculated upper and lower limits on k_d for the 360, 240, and 150 μm sands were 0.0174 to 0.0171, 0.0413 to 0.0404, and 0.0734 to 0.0718 min^{-1} , respectively. If we also consider a conservative estimate for the variation on the quartz zeta potential of -80 ± 10 mV (Redman et al., 2004), then the calculated upper and lower limits on k_d for the 360, 240, and 150 μm sands were only slightly changed to 0.0180 to 0.0166, 0.0426 to 0.0392, and 0.0759 to 0.0698 min^{-1} , respectively. In Fig. 6c it is apparent that values of k_d encompass a much larger range than predicted by either analysis. This observation indicates that heterogeneity of the colloid surface charge characteristics cannot fully account for the largest values of k_d that were shown in Fig. 6c and that were primarily responsible for deposition near the column inlet. Also, the fitted values of σ_d were dependent on the sand size (Table 1), with increasing values observed for the larger sands. If colloid heterogeneity was truly controlling the deposition behavior of the colloids, then the value of σ_d would be expected to be independent of the sand size.

An alternative approach to characterize the experimental data shown in Fig. 6a and 6b is to use the bimodal log-normal distribution for $F(k_d)$ according to Eq. [8] or [9]. Figures 6a and 6b also present simulated (Eq. [14–16]) breakthrough curves and deposition profiles, respectively, using

this approach. To minimize the number of fitting parameters, these simulations employed Eq. [9–11] and the value of k_{d2} was set to a high value ($0.3 min^{-1}$) that produced no colloid transport at the depth of 12 cm. Table 1 provides the fitted values of f_1 and k_{d1} , as well as a statistical parameters for the goodness of model fits. The simplified “stochastic” model provides a good description of both effluent and deposition data. Note in Table 1 that values of k_{d1} increased with decreasing sand size, and that values of f_1 decreased with decreasing sand size.

Previous researchers who have utilized bimodal formulations for $F(k_d)$ have attributed this distribution to charge variability of the colloids and/or porous media (Tufenkji and Elimelech, 2005a, 2005b). The calculated upper and lower limits on k_d discussed above, however, indicate that colloid charge heterogeneity cannot explain the observed hyperexponential deposition profiles for these experimental conditions. Alternative explanations for the hyperexponential deposition profiles shown in Fig. 6a and 6b include variability in the colloid size distribution, the pore-scale velocity distribution, and the pore size distribution. These topics will be discussed below.

If the colloids are not completely monodispersed, then colloids in the distribution are expected to have different deposition rates. Attachment (Tufenkji and Elimelech, 2004a) and straining (Bradford et al., 2003) of colloids are both predicted to increase with increasing size. If two size classes of colloids (monodispersed and aggregated species) are considered, and k_{d1} and k_{d2} correspond to deposition coefficients for monodispersed and aggregated species, then f_1 is equal to the ratio of monodispersed colloids to total colloids (in terms of monodispersed colloids) in the influent solution. According to this hypothesis the value of f_1 should be the same for the various sands in Fig. 6a and 6b. Table 1, however, indicates that the value of f_1 changes with the sand size and suggests that variations in the colloid size distribution cannot fully explain the observed transport and deposition behavior of these colloids. Furthermore, the colloid size distribution was experimentally verified using a laser particle size distribution analyzer to be monodispersed.

Figures 2 and 5 indicate that variations in the pore water velocity provide an alternative explanation for hyperexponen-

Table 1. Experimental and simulated model parameters for the data shown in Fig. 6a–c, as well as statistical parameters for the goodness of model fit. The value of k_1 was set to $0.0001 min^{-1}$ in all cases.

Model	d_{50}^\dagger μm	ϵ	v $cm min^{-1}$	D $cm^2 min^{-1}$	$\langle k_d \rangle$ min^{-1}	σ_d	r_{eff}^2	r_{sand}^2	f_1	k_{d1}	k_{d2}
										— min^{-1} —	
Log-normal	360	0.35	0.274	0.197	0.045	2.0	0.90	0.82			
Log-normal	240	0.32	0.325	0.085	0.085	1.0	0.94	0.89			
Log-normal	150	0.35	0.274	0.079	0.120	0.8	0.87	0.87			
Bimodal	360	0.35	0.274	0.197			0.90	0.90	0.90	0.007	0.30
Bimodal	240	0.32	0.325	0.085			0.94	0.98	0.57	0.027	0.30
Bimodal	150	0.35	0.274	0.079			0.86	0.99	0.37	0.032	0.30

$^\dagger d_{50}$, median porous medium grain diameter (L); ϵ , denotes porosity; v , average pore water velocity ($L T^{-1}$); D , hydrodynamic dispersion coefficient ($L^2 T^{-1}$); k_d , deposition coefficient (T^{-1}); σ_d , standard deviation for the deposition coefficient of the log-normal probability density function; r_{eff}^2 , coefficient of linear regression to effluent data; r_{sand}^2 , coefficient of linear regression to deposition data; f_1 , fraction of k_d that is assigned to log-normal distribution 1; k_{d1} , deposition coefficient in distribution 1 when $\sigma_{d1} = 0$; k_{d2} , deposition coefficients in distribution 2 when $\sigma_{d2} = 0$.

tial profiles than solely chemical heterogeneity. The stochastic stream tube model represents the complex three-dimensional flow field in porous media by a bundle of one-dimensional stream tubes of equal length. In homogeneous porous media it may be possible to estimate a pore water velocity distribution from measuring capillary pressure curves by assuming LaPlace's equation of capillarity and Poiseuille flow in the capillary tubes (Dullien, 1992). Although large variations in pore sizes are frequently measured in porous media (e.g., Dane and Hopmans, 2002), this analysis is likely to be based on assumptions that may be violated. For example, the stream tube model does not account for mixing of colloids among the stream tubes, and soil pores have more complex shapes than capillary tubes. Hence, consideration of only pore-scale velocity variations is likely to have limited utility.

Recent experimental evidence indicates that the deposition rates (under unfavorable attachment conditions) in the smallest regions of the pore space are significantly higher than in the larger regions of the pore space because these locations are associated with lower flow velocities (regions of relative flow stagnation that are associated with less fluid drag forces) (Johnson et al., 2007), greater DLVO forces (Hoek and Agarwal, 2006), and the presence of multiple solid-water interfaces (small pore spaces) that impose a physical restriction on colloid transport and enhance deposition (i.e., straining) in these locations (Bradford et al., 2006a). According to this conceptual picture, variations in the stochastic model parameters can be given a different interpretation than solely chemical heterogeneity or variations in the pore water velocity. For example, fitted values of $F(k_d)$ can be viewed as representing a complex coupling of pore-scale colloid mass transfer, hydrodynamics, and DLVO interactions within the pore space. The log-normal probability density function for $F(k_d)$ suggests a trend of gradually increasing retention of colloids in the largest (highly conductive pore bodies) to the smallest (lower conductivity pore corners formed at grain to grain contacts) regions of the pore space. In contrast, the bimodal formation for $F(k_d)$ suggests an abrupt increase in deposition behavior in the smaller regions of the pore space. The rapid change in shape of the deposition profiles near the column entrance shown in Fig. 6b suggests that the bimodal formation for $F(k_d)$ was more consistent with this data than the log-normal $F(k_d)$. The values of r_s^2 in Table 1 also support this hypothesis.

Physically realistic functional forms for $F(k_d)$ are expected to be dependent on a balance of DLVO and fluid drag forces (Cushing and Lawler, 1998), as well as the ratio of the colloid to the median grain size of a porous medium (Bradford et al., 2006a). Increasing the DLVO forces will increase this "favorable" deposition region for given hydrodynamic conditions. Increasing the colloid size or decreasing the median grain size of a porous medium will also increase the fraction of the pore space that is similar in size to a given colloid, and where colloids can be physically retained via straining. Conversely, increasing the fluid drag forces (velocity) decreases the low velocity region of the pore space that is "favorable" for deposition for given DLVO forces.

The stochastic model presented herein is intended to provide a tool to better understand and to test hypotheses concerning colloid transport and deposition under unfavorable attachment

conditions. The simulations presented in this manuscript suggest that various explanations can account for hyperexponential deposition profiles, including variations in the colloid surface charge, colloid size distribution, pore water velocity distribution, and pore size distribution. It is plausible that all of these factors influence the development of colloid deposition profiles under unfavorable attachment conditions. Specific tests can be performed to assess the relative importance of some of these factors. For example, charge heterogeneity can be assessed by measuring colloid zeta potential distributions, and/or by measuring differences in the colloid zeta potential distribution before and after passage through porous media. Colloid size distributions can also be measured using conventional particle size distribution analyzers and/or by microscopic examination of suspensions. Pore size and velocities distribution for porous media may be inferred from measured capillary pressure-saturation curves (Bradford et al., 2006a). To better predict values of $F(k_d)$ in porous media, all of this information likely needs to be coupled with DLVO and fluid drag force balances.

Acknowledgments

This research was supported by the 206 Manure and Byproduct Utilization Project of the USDA-ARS and in part by the grants from NRI and EPA (NRI #:2006-02541 and EPA IAG # DW-12-92189901-0). The authors would also like to thank Drs. Jirka Simunek, Martinus Th. van Genuchten, Saeed Torkzaban, and Sharon Walker for helpful discussions related to this manuscript. Mention of trade names and company names in this manuscript does not imply any endorsement or preferential treatment by the USDA.

References

- Albinger, O., B.K. Biesemeyer, R.G. Arnold, and B.E. Logan. 1994. Effect of bacterial heterogeneity on adhesion to uniform collectors by monoclonal populations. *FEMS Microbiol. Lett.* 124:321–326.
- Baygents, J.C., J.R. Glynn, Jr., O. Albinger, B.K. Biesemeyer, K.L. Ogden, and R.G. Arnold. 1998. Variation of surface charge density in monoclonal bacterial populations: Implications for transport through porous media. *Environ. Sci. Technol.* 32:1596–1603.
- Bekhit, H.M., and A.E. Hassan. 2005. Stochastic modeling of colloid-contaminant transport in physically and geochemically heterogeneous porous media. *Water Resour. Res.* 41(2), Art. No. W02010.
- Bergendahl, J., and D. Grasso. 1999. Prediction of colloid detachment in a model porous media: Thermodynamics. *AIChE J.* 45:475–484.
- Bolster, C.H., A.L. Mills, G.M. Hornberger, and J.S. Herman. 1999. Spatial distribution of deposited bacteria following miscible displacement experiments in intact cores. *Water Resour. Res.* 35:1797–1807.
- Bolster, C.H., A.L. Mills, G.M. Hornberger, and J.S. Herman. 2000. Effect of intra-population variability on the long-distance transport of bacteria. *Ground Water* 38:370–375.
- Bradford, S.A., and M. Bettahar. 2005. Straining, attachment, and detachment, of *Cryptosporidium* oocysts in saturated porous media. *J. Environ. Qual.* 34:469–478.
- Bradford, S.A., M. Bettahar, J. Simunek, and M.Th. van Genuchten. 2004. Straining and attachment of colloids in physically heterogeneous porous media. *Vadose Zone J.* 3:384–394.
- Bradford, S.A., J. Simunek, M. Bettahar, Y.F. Tadassa, M.Th. van Genuchten, and S.R. Yates. 2005. Straining of colloids at textural interfaces. *Water Resour. Res.* 41, Art. No. W10404, doi:10.1029/2004WR003675.
- Bradford, S.A., J. Simunek, M. Bettahar, M.Th. van Genuchten, and S.R. Yates. 2003. Modeling colloid attachment, straining, and exclusion in saturated porous media. *Environ. Sci. Technol.* 37:2242–2250.

- Bradford, S.A., J. Simunek, M. Bettahar, M.Th. van Genuchten, and S.R. Yates. 2006a. Significance of straining in colloid deposition: Evidence and implications. *Water Resour. Res.* 42, W12S15, doi:10.1029/2005WR004791.
- Bradford, S.A., J. Simunek, and S.L. Walker. 2006b. Transport and straining of *E. coli* O157:H7 in saturated porous media. *Water Resour. Res.* 42, W12S12, doi:10.1029/2005WR004805.
- Bradford, S.A., S. Torkzaban, and S.L. Walker. 2007. Coupling of physical and chemical mechanisms of colloid straining in saturated porous media. *Water Res.* (in press).
- Bradford, S.A., S.R. Yates, M. Bettahar, and J. Simunek. 2002. Physical factors affecting the transport and fate of colloids in saturated porous media. *Water Resour. Res.* 38, Art. No. 1327, doi:10.1029/2002WR001340.
- Camesano, T.A., and B.E. Logan. 1998. Influence of fluid velocity and cell concentration on the transport of motile and nonmotile bacteria in porous media. *Environ. Sci. Technol.* 32:1699–1708.
- Corapcioglu, M.Y., and H. Choi. 1996. Modeling colloid transport in unsaturated porous media and validation with laboratory column data. *Water Resour. Res.* 32:3437–3449.
- Cushing, R.S., and D.F. Lawler. 1998. Depth filtration: Fundamental investigation through three-dimensional trajectory analysis. *Environ. Sci. Technol.* 32:3793–3801.
- Dane, J.H., and J.W. Hopmans. 2002. Water retention and storage. *In* J.H. Dane and G.C. Topp (ed.) *Methods of soil analysis: Part 4. Physical methods*. SSSA, Madison, WI.
- Davis, J.A. 1982. Adsorption of dissolved natural organic matter at the oxide/water interface. *Geochim. Cosmochim. Acta* 46:2381–2393.
- DeFlaun, M.F., C.J. Murray, M. Holben, T. Scheibe, A. Mills, T. Ginn, T. Griffin, E. Majer, and J.L. Wilson. 1997. Preliminary observations on bacterial transport in a coastal plain aquifer. *FEMS Microbiol. Rev.* 20:473–487.
- Derjaguin, B.V., and L.D. Landau. 1941. Theory of the stability of strongly charged lyophobic sols and of the adhesion of strongly charged particles in solutions of electrolytes. *Acta Physicochim. USSR* 14:733–762.
- Dong, H., T.C. Onstott, C.-H. Ko, A.D. Hollingsworth, D.G. Brown, and B.J. Mailloux. 2002. Theoretical prediction of collision efficiency between adhesion-deficient bacteria and sediment grain surface. *Colloids Surf., B* 24:229–245.
- Dullien, F.A.L. 1992. *Porous media: Fluid transport and pore structure*. Academic Press, San Diego, CA.
- Elimelech, M., M. Nagai, C.-H. Ko, and J.N. Ryan. 2000. Relative insignificance of mineral grain zeta potential to colloid transport in geochemically heterogeneous porous media. *Environ. Sci. Technol.* 34:2143–2148.
- Foppen, J.W.A., A. Mporokoso, and J.F. Schijven. 2005. Determining straining of *Escherichia coli* from breakthrough curves. *J. Contam. Hydrol.* 76:191–210.
- Gregory, J. 1981. Approximate expression for retarded van der Waals interaction. *J. Colloid Interface Sci.* 83:138–145.
- Hahn, M.W., D. Abadzic, and C.R. O'Melia. 2004. Aquasols: On the role of secondary minima. *Environ. Sci. Technol.* 38:5915–5924.
- Harvey, R.W., and S.P. Garabedian. 1991. Use of colloid filtration theory in modeling movement of bacteria through a contaminated sandy aquifer. *Environ. Sci. Technol.* 25:178–185.
- Hoek, E.M.V., and G.K. Agarwal. 2006. Extended DLVO interactions between spherical particles and rough surfaces. *J. Colloid Interface Sci.* 298:50–58.
- Hogg, R., T.W. Healy, and D.W. Fuerstenau. 1966. Mutual coagulation of colloidal dispersions. *Trans. Faraday Soc.* 62:1638–1651.
- Johnson, P.R., and M. Elimelech. 1995. Dynamics of colloid deposition in porous media: Blocking based on random sequential adsorption. *Langmuir* 11:801–812.
- Johnson, W.P., and X. Li. 2005. Comment on “Breakdown of colloid filtration theory: Role of secondary energy minimum and surface charge heterogeneities”. *Langmuir* 21:10896–10897.
- Johnson, W.P., X. Li, and S. Assemi. 2006. Deposition and re-entrainment dynamics of microbes and non-biological colloids during non-perturbed transport in porous media in the presence of an energy barrier to deposition. *Adv. Water Res.* (in press).
- Jury, W.A., and K. Roth. 1990. *Transfer functions and solute movement through soil: Theory and applications*. Birkhauser Verlag, Basel, Switzerland.
- Kretzschmar, R., K. Barmettler, D. Grolimund, Y.D. Yan, M. Borkovec, and H. Sticher. 1997. Experimental determination of colloid deposition rates and collision efficiencies in natural porous media. *Water Resour. Res.* 33:1129–1137.
- Johnson, W.P., X. Li, and G. Yal. 2007. Colloid retention in porous media: Mechanistic confirmation of wedging and retention in zones of flow stagnation. *Environ. Sci. Technol.* (in press).
- Li, X., T.D. Scheibe, and W.P. Johnson. 2004. Apparent decreases in colloid deposition rate coefficient with distance of transport under unfavorable deposition conditions: A general phenomenon. *Environ. Sci. Technol.* 38:5616–5625.
- Li, X., P. Zhang, C.L. Lin, and W.P. Johnson. 2005. Role of hydrodynamic drag on microsphere deposition and re-entrainment in porous media under unfavorable conditions. *Environ. Sci. Technol.* 39:4012–4020.
- Liu, D., P.R. Johnson, and M. Elimelech. 1995. Colloid deposition dynamics in flow-through porous media: Role of electrolyte concentration. *Environ. Sci. Technol.* 29:2963–2973.
- Logan, B.E., D.G. Jewett, R.G. Arnold, E.J. Bouwer, and C.R. O'Melia. 1995. Clarification of clean-bed filtration models. *J. Environ. Eng.* 121:869–873.
- Maxwell, R.M., C. Welty, and A.F.B. Tompson. 2003. Streamline-based simulation of virus transport resulting from long term artificial recharge in a heterogeneous aquifer. *Adv. Water Resour.* 26:1075–1096.
- Rajagopalan, R., and C. Tien. 1976. Trajectory analysis of deep-bed filtration with the Sphere-in-Cell porous-media model. *AIChE J.* 22:523–533.
- Redman, J.A., S.B. Grant, T.M. Olson, and M.K. Estes. 2001. Pathogen filtration, heterogeneity, and the potable reuse of wastewater. *Environ. Sci. Technol.* 35:1798–1805.
- Redman, J.A., S.L. Walker, and M. Elimelech. 2004. Bacterial adhesion and transport in porous media: Role of the secondary energy minimum. *Environ. Sci. Technol.* 38:1777–1785.
- Rehmann, L.L.C., C. Welty, and R.W. Harvey. 1999. Stochastic analysis of virus transport in aquifers. *Water Resour. Res.* 35:1987–2006.
- Ryan, J.N., and M. Elimelech. 1996. Colloid mobilization and transport in groundwater. *Colloids Surf., A* 107:1–56.
- Ryan, J.N., M. Elimelech, R.A. Ard, R.W. Harvey, and P.R. Johnson. 1999. Bacteriophage PRD1 and silica colloid transport and recovery in an iron oxide-coated sand aquifer. *Environ. Sci. Technol.* 33:63–73.
- Schijven, J.K., and S.M. Hassanizadeh. 2000. Removal of viruses by soil passage: Overview of modeling, processes, and parameters. *Crit. Rev. Environ. Sci. Technol.* 30:49–127.
- Simoni, S.F., H. Harms, T.N.P. Bosma, and A.J.B. Zehnder. 1998. Population heterogeneity affects transport of bacteria through sand columns at low flow rates. *Environ. Sci. Technol.* 32:2100–2105.
- Song, L., and M. Elimelech. 1993. Dynamics of colloid deposition in porous media: Modeling the role of retained particles. *Colloids Surf., A* 73:49–63.
- Song, L., and M. Elimelech. 1994. Transient deposition of colloidal particles in heterogeneous porous media. *J. Colloid Interface Sci.* 167:301–313.
- Tan, Y., J.T. Cannon, P. Baveye, and M. Alexander. 1994. Transport of bacteria in an aquifer sand—Experiments and model simulations. *Water Resour. Res.* 30:3243–3252.
- Tipping, E., and D. Cooke. 1982. The effects of adsorbed humic substances on the surface charge of goethite in freshwaters. *Geochim. Cosmochim. Acta* 46:75–80.
- Tong, M., and W.P. Johnson. 2007. Colloid population heterogeneity drives hyper-exponential deviation from classic filtration theory. *Environ. Sci. Technol.* 41(2):493–499.
- Tong, M., X. Li, C.N. Brow, and W.P. Johnson. 2005. Detachment-influenced transport of an adhesion-deficient bacterial strain within water-reactive porous media. *Environ. Sci. Technol.* 39:2500–2508.
- Toride, N., F.J. Leij, and M.Th. van Genuchten. 1995. The CXTFIT code for estimating transport parameters from laboratory and field tracer experiments. *Research Rep. No. 137*, U.S. Salinity Lab., ARS, USDA, Riverside, CA.
- Tufenkji, N., J.A. Redman, and M. Elimelech. 2003. Interpreting deposition patterns of microbial particles in laboratory-scale column experiments. *Environ. Sci. Technol.* 37:616–623.
- Tufenkji, N., G.F. Miller, J.N. Ryan, R.W. Harvey, and M. Elimelech. 2004. Transport of *Cryptosporidium* oocysts in porous media: Role of straining and physicochemical filtration. *Environ. Sci. Technol.* 38:5932–5938.
- Tufenkji, N., and M. Elimelech. 2004a. Correlation equation for predicting single-collector efficiency in physicochemical filtration in saturated porous media. *Environ. Sci. Technol.* 38:529–536.
- Tufenkji, N., and M. Elimelech. 2004b. Deviation from the classical colloid filtration theory in the presence of repulsive DLVO interactions. *Langmuir* 20:10818–10828.
- Tufenkji, N., and M. Elimelech. 2005a. Breakdown of colloid filtration

theory: Role of the secondary energy minimum and surface charge heterogeneities. *Langmuir* 21:841–852.

Tufenkji, N., and M. Elimelech. 2005b. Spatial distributions of *Cryptosporidium* oocysts in porous media: Evidence for dual mode deposition. *Environ. Sci. Technol.* 39:3620–3629.

Verwey, E.J.W., and J.Th.G. Overbeek. 1948. *Theory of the stability of lyophobic colloids*. Elsevier, Amsterdam.

Yao, K.M., M.T. Habibian, and C.R. O'Melia. 1971. Water and waste water filtration—Concepts and applications. *Environ. Sci. Technol.* 5:1105–1112.

Zhang, P., W.P. Johnson, T.D. Scheibe, K. Choi, F.C. Dobbs, and B.J. Mailloux. 2001. Extended tailing of bacteria following breakthrough at the Narrow Channel Focus Area, Oyster, Virginia. *Water Resour. Res.* 37:2687–2698.

Appendix

C	colloid concentration in the aqueous phase ($N_c \text{ L}^{-3}$)
C_i	initial colloid concentration in the influent suspension ($N_{ic} \text{ L}^{-3}$)
d_{50}	median porous medium grain diameter (L)
D	hydrodynamic dispersion coefficient ($\text{L}^2 \text{ T}^{-1}$)
E	kinetic energy of diffusing colloids that follow a Maxwell distribution ($\text{M L}^2 \text{ T}^{-2}$)
f_1	fraction of k_d that is assigned to log-normal distribution 1
$F(x)$	log-normal probability density function for dummy variable x
$F(x,y)$	joint probability density function for dummy variables x and y
k_b	Boltzmann constant ($\text{M L}^2 \text{ T}^{-2} \text{ }^\circ\text{K}^{-1}$)
k_d	deposition coefficient (T^{-1})
k_{d1}	deposition coefficient in distribution 1 when $\sigma_{d1} = 0$ (T^{-1})
k_{d2}	deposition coefficients in distribution 2 when $\sigma_{d2} = 0$ (T^{-1})
k_r	release coefficient (T^{-1})
L	denotes units of length
M	denotes units of mass
N_c	number of colloids
N_{ic}	number of colloids in a unit volume of C_i
S	solid phase concentration of the retained colloids ($N_c \text{ M}^{-1}$)
t	time (T)
T_k	temperature in degrees Kelvin ($^\circ\text{K}$)
v	average pore water velocity (L T^{-1})
Y_d	normalized log-transformed variable for the deposition coefficient
Y_{d1}	normalized log-transformed variable for the distribution 1 deposition coefficient of the bimodal log-normal probability density function
Y_{d2}	normalized log-transformed variable for the distribution 2 deposition coefficient of the bimodal log-normal probability density function
Y_r	normalized log-transformed variable for the release coefficient
Y_v	normalized log-transformed variable for the pore water velocity
z	depth (L)
α	colloid sticking efficiency
Γ	gamma function
Γ_i	incomplete gamma function
δ	Dirac delta function
η	collector (porous medium) efficiency
θ_w	volumetric water content
μ_d	mean value for the deposition coefficient of the log-normal probability density function
μ_r	mean value for the release coefficient of the log-normal probability density function
μ_v	mean value for the pore water velocity of the log-normal probability density function
μ_{d1}	mean value of the distribution 1 deposition coefficient of the bimodal log-normal probability density function
μ_{d2}	mean value of the distribution 2 deposition coefficient of the bimodal log-normal probability density function
ρ_b	soil bulk density (M L^{-3})
ρ_{dr}	correlation coefficient between Y_d and Y_r
ρ_{vd}	correlation coefficient between Y_v and Y_d
σ_d	standard deviation for the deposition coefficient of the log-normal probability density function
σ_{d1}	standard deviation for the distribution 1 deposition coefficient of the bimodal log-normal probability density function
σ_{d2}	standard deviation for the distribution 2 deposition coefficient of the bimodal log-normal probability density function
σ_r	standard deviation for the release coefficient of the log-normal probability density function
σ_v	standard deviation for the pore water velocity of the log-normal probability density function
Φ_2	depth of the secondary energy minimum of the DLVO interaction energy profile that is normalized by $k_b T_k$
$\langle x \rangle$	ensemble average of a dummy variable x
